Array Shading to Maximize Deflection Coefficient for Broadband Signal Detection With Conventional Beamforming

KAUSHALLYA ADHIKARI [1], **(Member, IEEE), BLAINE M. HARKER**[2],
THOMAS A. WETTERGREN[2], **(Senior Member, IEEE),**
LAUREN A. FREEMAN[2], **AND SIMON E. FREEMAN**[2]

[1]Department of Electrical, Computer, and Biomedical Engineering, University of Rhode Island, Kingston, RI 02881, USA
[2]Naval Undersea Warfare Center, Newport, RI 02841, USA

Corresponding author: Kaushallya Adhikari (kadhikari@uri.edu)

ABSTRACT This paper develops and applies a numerical optimization procedure to compute broadband noise-adaptive weights for delay and sum beamforming that are conditioned to maximize the deflection coefficient at the output of a square law detector for a given set of underwater pressure measurements. The resulting optimal weights mitigate the effects of noise and interferers and maximize signal detection. Comparison of the optimal weights with minimum variance distortionless response weights show that the presented algorithm provides higher attenuation of interferers. We also use the noise-adaptive algorithm to find the optimal sparse array geometry for a given number of sensors and aperture. Comparison of the resulting optimal array with coprime, nested, and semi-coprime arrays shows that the proposed sparse array suppresses interferers more than the other sparse arrays.

INDEX TERMS Conventional beamforming, deflection coefficient, delay and sum beamforming, detection statistic, Gaussian distribution, signal detection.

I. INTRODUCTION

Delay-and-sum beamforming (DSB) is the oldest beamforming algorithm and it persists as a preferable and powerful approach today because of its simplicity and robustness—other approaches are very sensitive [1]. As its name states, DSB works by delaying the shaded sensor outputs and summing the outputs to reinforce signals from a desired direction (coherent addition), while averaging out noise (incoherent addition). The DSB is also referred to as conventional beamforming (CBF) [2] and we use the terms DSB and CBF interchangeably in the sequel. The shading weights, in general, are selected by considering the trade-off between the mainlobe width and peak sidelobe height of the beampattern associated with the shading. Since the parameters of DSB algorithms do not depend on data, they cannot take advantage of the signal and noise characteristics. An additional category of beamformers, known as adaptive beamformers, calculate shading weights based on the characteristics of the observations. These beamformers

yield signal detection and estimation performance that exceed those of DSB algorithms; although they are tuned to specific observations and thus need to be re-computed for changes in the observations. The minimum variance distortionless response (MVDR) beamformer is an adaptive beamformer, which is popular owing to its high resolution and effectiveness in suppressing noise and interferers [1], [2]. However, the MVDR beamformer requires inversion of the sample covariance matrix (SCM), which can be challenging in underwater scenarios that are non-stationary and snapshot-deficient.

Wettergren *et al.* developed noise-adaptive delay-and-sum beamforming (NADSB) that preserves the simplicity of classical DSB but adapts its parameters to observations without having to invert an SCM [3]–[5]. The NADSB algorithm implemented in [3] finds the array weights that maximize the deflection coefficient at the input of the square-law detector, while the NADSB algorithm implemented in [4], [5] maximizes the deflection coefficient at the output of the square-law detector. In each case, a single set of weights is computed independent of frequency as opposed to weights calculated for each narrowband frequency as is typically

The associate editor coordinating the review of this manuscript and approving it for publication was Irfan Ahmed [ID].

performed. The array weights are functions of either modeled or observed structural noise and are optimized to mitigate the effect of noise on weak broadband signal detection. The algorithm was previously applied to conformal velocity sonar data to determine optimal weights for time-domain DSB.

In this work, we maximized the deflection coefficient at the output of the square-law detector as the optimality criterion and applied the NADSB algorithm to array ambient noise measurements collected off the coast of Hawaii using a linear array. We also formulated the NADSB algorithm to find the optimal sensor locations for sparse arrays with a given aperture and number of sensors. We compared the optimal sparse arrays with standard sparse arrays such as coprime arrays, nested arrays, and semi-coprime arrays [6], [7]. Our specific contributions are:

1) Application of the NADSB algorithm to the underwater data obtained from a linear array of sensors and comparison of the results with MVDR.
2) Derivation of the analytical expression for optimal shading when the noise measurements are uncorrelated.
3) Formulation of the NADSB algorithm to find the optimal sparse array for a given aperture and number of sensors.

Section II describes the signal model. Section II-B provides a brief review of the related work. Section III describes the NADSB algorithm. Section IV provides examples of numerical evaluation of the optimal weights. Section V finds optimal sparse array configurations for a given aperture and number of sensors. Section VI finds optimal shading for standard sparse arrays. Section VII summarizes the paper's contributions.

Notations: Boldfaced lowercase math symbols denote vectors and boldfaced uppercase math symbols denote matrices. $\mathbf{x}^T$ denotes transpose of $\mathbf{x}$. x^* denotes complex conjugate of x. $\mathbf{x}^H$ denotes Hermitian (conjugate-transpose) of $\mathbf{x}$. $\mathbf{I}_L$ is an L-by-L identity matrix. $\mathbf{1}_L$ is an L-by-1 vector of all ones. $\mathbf{0}_L$ is an L-by-1 vector of all zeroes. $\mathfrak{D}\{\mathbf{A}\}$ denotes the vector containing the diagonal elements of $\mathbf{A}$. $\mathcal{D}\{\mathbf{a}\}$ denotes the diagonal matrix with the operands $\mathbf{a}$ along the diagonal of the matrix. $\mathcal{S}\{\mathbf{a}\}$ denotes the sum of the elements of $\mathbf{a}$. $\mathbb{E}\{a\}$ denotes the expected value of a and $\mathbb{V}\{a\}$ denotes the variance of a. $\mathbf{a} \sim \mathcal{N}_L(\boldsymbol{\mu}, \mathbf{R})$ means $\mathbf{a}$ is an L-by-1 random vector with normal distribution with mean $\boldsymbol{\mu}$ and covariance matrix $\mathbf{R}$.

II. RECEIVED SIGNAL MODEL

We consider a passive sonar detection problem consisting of a broadband plane-wave acoustic signal incoming at spherical angles (θ_0, ϕ_0). The signal is propagated to each array sensor position–which measures the signal as well as ambient acoustic noise–and sensor self noise. The composite signal received by the array of sensors can be regarded as a random signal in noise [8]. For a detection problem, the suitable model for the data measured by an array of L sensors is

$$H_1 : \mathbf{y}(t) = \mathbf{s}(t) + \mathbf{n}(t) \tag{1}$$

if the signal of interest is present and

$$H_0 : \mathbf{y}(t) = \mathbf{n}(t) \tag{2}$$

if it is not, where $\mathbf{y}(t)$, $\mathbf{s}(t)$, and $\mathbf{n}(t)$ are each L-by-1 vectors. The signal vector $\mathbf{s}(t)$ and the noise vector $\mathbf{n}(t)$ are samples of random vectors and they are uncorrelated. Any detection procedure for such a model involves a hypothesis test between the two above models, which has to be based on the statistical properties of these underlying random vectors [8]. The array measurements in both hypotheses can be regarded as samples of Gaussian vectors, owing to the central limit theorem [9]:

$$H_1 : \mathbf{y}(t) \sim \mathcal{N}_L\left(\mathbf{0}_L, \mathbf{K}_y = \mathbf{K}_s + \mathbf{K}_n\right) \tag{3}$$

and

$$H_0 : \mathbf{y}(t) \sim \mathcal{N}_L\left(\mathbf{0}_L, \mathbf{K}_y = \mathbf{K}_n\right), \tag{4}$$

where the matrices $\mathbf{K}_y$, $\mathbf{K}_s$, and $\mathbf{K}_n$ are the covariances of $\mathbf{y}(t)$, $\mathbf{s}(t)$, and $\mathbf{n}(t)$, respectively.

The beamforming procedure takes the measured data $\mathbf{y}(t)$ and forms a linear weighted combination to create a beam-formed output $z(t)$. The output of the DSB or CBF steered to spherical coordinates (θ, ϕ) is $z(t) = \mathbf{w}^T \tilde{\mathbf{y}}(t)$, where $\mathbf{w} = [w_1, w_2, \ldots, w_L]^T$ is the weight vector that includes the array amplitude shading, $\tilde{\mathbf{y}}(t) = \mathbf{y}(t - \Delta_m)$ and Δ_m is the time delay required for the mth sensor. Since the beamforming procedure is a linear transformation from $\tilde{\mathbf{y}}(t)$ to $z(t)$, the beamformer output also has Gaussian distribution, $z(t) \sim \mathcal{N}_1(0, \sigma_z^2)$. The detection statistic, $x(t)$, is the square of the beamformer output $x(t) = z^2(t)$, which has a central Chi-square distribution. The probability density function (PDF) of the detection statistic is [10]

$$f_X(x(t)) = \frac{1}{\sqrt{2\pi \sigma_z^2 x(t)}} \exp\left(-\frac{x(t)}{2\sigma_z^2}\right). \tag{5}$$

The associated scalar version of the hypothesis testing problem becomes:

$$H_1 : x(t) = z^2(t), \text{ where } z(t) \sim \mathcal{N}_1(0, \sigma_{z1}^2) \tag{6}$$

and

$$H_0 : x(t) = z^2(t), \text{ where } z(t) \sim \mathcal{N}_1(0, \sigma_{z0}^2). \tag{7}$$

The covariances σ_{z1}^2 and σ_{z0}^2 correspond to alternate and null hypotheses cases, respectively.

A. DEFLECTION COEFFICIENT

In a binary hypothesis testing problem, where the detection statistic is $x(t)$, the deflection coefficient is defined as

$$d = \frac{\mathbb{E}\{x(t)|H_1\} - \mathbb{E}\{x(t)|H_0\}}{\sqrt{\mathbb{V}\{x(t)|H_0\}}} \tag{8}$$

[8], [11]. When both alternate and null hypotheses are Gaussian distributed with different means but equal variances, the deflection coefficient completely characterizes the detection performance. This is because the deflection coefficient determines the ability of an optimal hypothesis test to make

a decision as to which Gaussian distribution might have generated the observed value of $x(t)$ [11], [12]. In other problems where the two distributions are not simply Gaussian distributed with different means, the deflection coefficient is used for approximate detection performance [11], [13], [14]. Therefore, we consider maximizing deflection coefficient to optimize the detection performance.

B. A REVIEW OF THE RELATED WORK
This section briefly summarizes the prior related work in [3]–[5].

1) DEFLECTION COEFFICIENT MAXIMIZATION AT THE OUTPUT OF A CONVENTIONAL BEAMFORMER TO OBTAIN SHADING WEIGHTS
A numerical approach of optimizing array shading weights for passive broadband detection was developed in [3] for acoustic hull arrays. The authors minimized the impact of modeled and measured noise sources on detection at a conventional beamformer output, maintaining the array gain against an unknown signal source. This was accomplished by maximizing the deflection coefficient at the output of a conventional beamformer, which is given by $d_1 = (\mu_{sN} - \mu_N)/\sigma_N$. The variables μ_{SN} and μ_N represent the mean values of the beamformer output for alternate and null hypotheses and σ_N represents the standard deviation of the beamformer output for null hypothesis. Denoting the beamformer output power spectra for the alternate and null hypotheses by $P_{SN}(\omega)$ and $P_N(\omega)$, respectively, the authors in [3] show that the deflection coefficient can be simplified to

$$d_1 = \frac{0.5\sqrt{T/\pi} \int_{-\infty}^{\infty} P_S(\omega)d\omega}{[\int_{-\infty}^{\infty} P_N^2(\omega)d\omega]^{\frac{1}{2}}}, \tag{9}$$

where T is the system averaging time and $P_S(\omega) = P_{SN}(\omega) - P_N(\omega)$. When the array is steered to the incident plane wave's direction of arrival, the signal only power spectrum at the beamformer output becomes $P_S(\omega) = F_S(\omega)\left(\sum_{m=1}^{M} w_m\right)^2$, where $F_S(\omega)$ is the power spectrum of the incident plane wave. By imposing the constraint $\sum_{m=1}^{M} w_m = 1$, the array gain for the plane wave in the steered direction is fixed. With this constraint, minimizing the denominator of (9) corresponds to maximization of the deflection coefficient at the output of the beamformer. To demonstrate the utility of this approach, [3] presents numerical results using modeled data for an 11-sensor uniform conformal array. Their results show higher gains compared to uniform shading for simple modeled noise sources.

2) DEFLECTION COEFFICIENT MAXIMIZATION AT THE OUTPUT OF A SQUARE-LAW DETECTOR TO OBTAIN SHADING WEIGHTS
The approach presented in [4], [5] improves upon the method developed in [3]. The authors in [4], [5] make the argument that maximizing the deflection coefficient at the output of

the square-law detector is more effective since the overall goal is to maximize detection performance. The deflection coefficient at the output of the square-law detector is [5]

$$d_2 = \sqrt{T\beta} \frac{\int_{-\infty}^{\infty} P_S(\omega)d\omega}{\int_{-\infty}^{\infty} P_N(\omega)d\omega}, \tag{10}$$

where $T\beta$ is the time-bandwidth product. The authors in [4], [5] maximize (10) by keeping the numerator fixed which corresponds to holding the signal response fixed in the look direction. When this method was applied to find the optimal shading weights for an 80-element conformal velocity sensor using real data, it resulted in 16 dB SNR improvement compared to uniform shading or Taylor shading.

Both of the DSB shading approaches shown in these sections (Section II-B1 and II-B2) use measurements of noise to tune conventional shading weights to improve detection performance. These have both been shown to lead to better detection than what is attainable with data-independent shading. The approach in Section II-B2 has the added advantage of directly optimizing performance at the output of the detector, and thus it has improved detection performance in practice. These approaches lead to identical array weights when the noise is white [5]. This is because $P_N(\omega)$ is a constant for white noise, which makes the denominators of (9) and (10) equal.

III. NADSB ALGORITHMS FOR A FULL ULA
We find the NADSB weights by maximizing the deflection coefficient at the output of the square-law detector, following the approach in Section II-B2. The objective function for maximization of the deflection coefficient has been derived in [4], [5]. We repeat the derivation here with slightly different notations and approach.

The beamformer output for the noise-only case is $z(t) = \sum_{m=1}^{L} w_m n_m(t - \Delta_m)$, where $n_m(t)$ is the measured noise at m^{th} sensor. The Fourier transform of $z(t)$ is $Z(\omega) = \sum_{m=1}^{L} w_m N_m(\omega) \exp(-j\omega\Delta_m)$, where $N_m(\omega)$ is the Fourier transform of $n_m(t)$. For each Δ_m, the product $\omega\Delta_m = \mathbf{k}_s.\mathbf{x}_m$, where $\mathbf{k}_s$ is the wavenumber vector and $\mathbf{x}_m$ is the mth sensor location [2, Chapter 2]. The frequency spectrum $Z(\omega)$ can be expressed using matrix notation as

$$Z(\omega) = \mathbf{w}^T \mathbf{U}^*(\omega)\mathbf{m}(\omega), \tag{11}$$

where $\mathbf{U} = \mathcal{D}\{e^{j\mathbf{k}_s.\mathbf{x}_1}, e^{j\mathbf{k}_s.\mathbf{x}_2}, \ldots, e^{j\mathbf{k}_s.\mathbf{x}_L}\}$ is the steering matrix for look direction corresponding to $\mathbf{k}_s$ and $\mathbf{m}(\omega) = [N_1(\omega), N_2(\omega), \ldots, N_L(\omega)]^T$. The noise power spectrum at the output of the beamformer is then given by

$$P_N(\omega) = |Z(\omega)|^2 = \mathbf{w}^T \mathbf{U}^*(\omega)\mathbf{m}(\omega)\mathbf{m}^H(\omega)\mathbf{U}(\omega)\mathbf{w}. \tag{12}$$

Denoting the L-by-L noise cross-power spectrum matrix $\mathbf{m}(\omega)\mathbf{m}^H(\omega)$ as $\mathbf{M}(\omega)$, we get

$$P_N(\omega) = \mathbf{w}^T \mathbf{U}^*(\omega)\mathbf{M}(\omega)\mathbf{U}(\omega)\mathbf{w}. \tag{13}$$

The row i, column j element of the cross-power spectrum matrix $\mathbf{M}(\omega)$ is the Fourier transform of the cross-correlation between $n_i(t)$ and $n_j(t)$. Therefore, for each i and j pair, we have

$$M_{ij}(\omega) = \int_{-\infty}^{\infty} \mathbb{E}\{n_i(t)n_j(t+\tau)\}e^{-j\omega\tau}\,d\tau. \quad (14)$$

Substituting (13) in the denominator of (10), we get the objective function $\mathbf{w}^T\left(\int_{\omega_1}^{\omega_2}\mathbf{U}^*(\omega)\mathbf{M}(\omega)\mathbf{U}(\omega)d\omega\right)\mathbf{w}$, where ω_1 and ω_2 are the minimum and maximum frequencies of interest. Therefore, maximization of the deflection coefficient at the output of the square law detector is equivalent to the following minimization problem

$$\min_{\mathbf{w}} \mathbf{w}^T\left(\int_{\omega_1}^{\omega_2}\mathbf{U}^*(\omega)\mathbf{M}(\omega)\mathbf{U}(\omega)d\omega\right)\mathbf{w}$$

$$\text{subject to } \Sigma_{m=1}^{L}w_m = 1 \text{ and } w_m \geq 0 \text{ for all } m. \quad (15)$$

For notational convenience, we represent the inner integral of (15) as

$$\mathbf{J} = \int_{\omega_1}^{\omega_2}\mathbf{U}^*(\omega)\mathbf{M}(\omega)\mathbf{U}(\omega)d\omega, \quad (16)$$

which is an L-by-L matrix.

Equations (15) and (16) were formulated in [4], [5] and solved numerically. In those prior works there were no cases presented for which an analytical solution was found. However, an analytical expression for the optimal weights can be derived when the noise measurements at the different sensors are uncorrelated, as shown in Section III-A. When the noise measurements are correlated, there is no analytical solution for the optimum and numerical optimization techniques must be used to find the optimal weights.

A. OPTIMAL WEIGHTS FOR UNCORRELATED NOISE

The minimization problem has a closed-form solution when there is zero correlation between different sensor pairs at all frequencies. This condition causes the matrix $\mathbf{M}(\omega)$ to be diagonal at every frequency and consequently, $\mathbf{J}$ is also a diagonal matrix. When $\mathbf{J}$ is a diagonal matrix, its mth diagonal element is the contribution to the total power by the mth sensor. Since we are considering a noise-only case (i.e. H_0 model), the diagonal element is the contribution to the total noise power level. Since the optimization problem is formulated to suppress the total noise, the optimal weights for various sensors are inversely proportional to the sensor noise power levels. The solution of the optimization problem (15) for uncorrelated noise can be written as

$$\mathbf{w}_{opt} = \frac{\mathfrak{D}\{\mathbf{J}^{-1}\}}{c_n}, \quad (17)$$

where c_n is the normalization constant given by the sum of the diagonal elements of $\mathbf{J}^{-1}$ (i.e., $c_n = \mathcal{S}\{\mathfrak{D}\{\mathbf{J}^{-1}\}\}$, where $\mathcal{S}\{.\}$ represents the sum of the elements of the operand). See Appendix A for full derivation.

When the noise measurements at different sensors are uncorrelated and the noise powers are equal, the diagonal

TABLE 1. Algorithm 1: Computation of the optimal weights.

Input:	$\mathbf{y}(t)$, for $t = t_1, t_2, ..., t_T$, where t_i is the ith observation time instant and T is the number of snapshots.
Output:	Optimal weights, $\mathbf{w}$
Step 1:	For a given dataset, compute each element of the noise cross-power spectrum using (14).
Step 2:	For a given look direction, compute the L-by-L matrix $\mathbf{J}$ using (16).
Step 3:	If $\mathbf{J}$ is diagonal, use (17) to find optimal $\mathbf{w}$. For non-diagonal $\mathbf{J}$, use the Sequential Quadratic Programming (SQP) solver *fmincon* [17] from the MATLAB optimization toolbox to numerically solve (15) to find optimal $\mathbf{w}$.
Step 4:	Repeat Steps 2 and 3 for each look direction.

elements of $\mathbf{J}$ are equal. In this case, the optimal shading in (17) is given by uniform shading. The NADSB algorithm, that applies to both correlated and uncorrelated noise, is summarized in Table 1.

## IV. NUMERICAL EVALUATION OF OPTIMAL WEIGHTS FOR A FULL ULA

In this section, we solve the minimization problem in (15) numerically using MATLAB-Optimization Toolbox [15]. The dataset used in this work is described in Section IV-A.

A. DATASET DESCRIPTION

A 128-element, tetrahedral hydrophone array (Figure 1) was deployed offshore of Kona, Hawaii at a depth of 23 m, for two cycles of continuous sampling. The array includes a 64-element ULA and two orthogonal 32-element ULAs; we used the 64-element ULA data in this project. Inter-element spacing was 170 mm, corresponding to an array design frequency of approximately 4.5 kHz (based on $\lambda/2$ spacing with sound speed for nominal water temperature). A 64-element linear stave and one 32-element orthogonal linear stave were deployed horizontally on the ocean floor while a second 32-element linear stave was deployed vertically. In the sequel, we will refer to the dataset from the 64-element linear array as the Kona dataset.

B. EVALUATION OF THE NOISE CROSS-POWER SPECTRUM MATRIX

The cross-power spectrum of noise measurements, $\mathbf{M}(\omega)$, were computed using the first 1-second of a dataset ranging from the frequency of 50 Hz to 4050 Hz. Figure 2 depicts the cross-power spectral density estimates among all pairs of sensors at various equally spaced temporal frequencies and it proves that the dataset contains spatially colored noise. The purpose of the NADSB algorithm is to exploit the spatial distribution of the noise field to reduce the impact of the noise field on weak signal detection over a broad range of temporal frequencies. Thus, the NADSB algorithm uses these cross-power spectral density estimates of the noise to tune the shading weights to the observed noise environment.
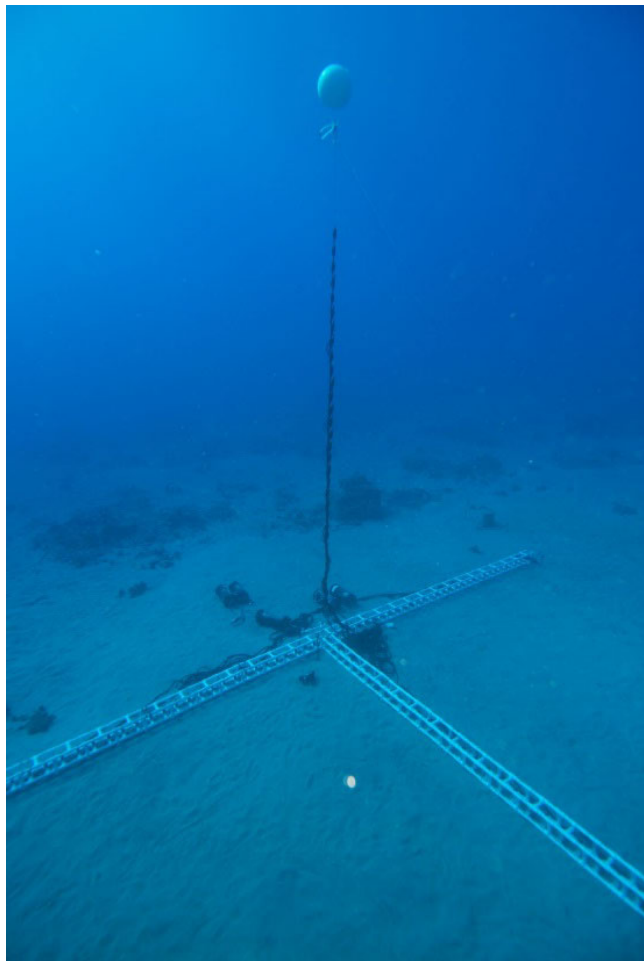
FIGURE 1. 128-element array deployed in Kona, HI. Array deployment includes a 64-element uniform line array and two orthogonal uniform arrays, each with 32 elements.

C. OPTIMAL WEIGHTS FOR A FULL ULA

Figure 3 depicts the optimal weights obtained for 181 different look directions. The look direction ranges from 0° to 180° in 1° increments. The figure demonstrates that there is minimal variation in the optimal weights with the look direction. The sensors that are weighted heavily (lightly), remain heavily (lightly) weighted across the range of look directions. Figure 4 provides an insight into the algorithm that optimizes the deflection coefficient at the output of the square law detector. The algorithm consistently assigns large weights to sensors 37 and 54 and negligibly small weights to all other sensors. The noise power levels at the outputs of sensors 37 and 54 are substantially less than the power levels at the outputs of the other sensors, as illustrated by Figure 4. The algorithm determines sensors 37 and 54 as the least noisy sensors and in an attempt to minimize the total noise power, assigns most of the weight to the two sensors. Since the algorithm considers the remaining 62 sensors as much noisier, it assigns approximately zero weights to the 62 sensors. However, sensors 37 and 54 were actually non-functional sensors and assigning disproportionately higher weights to

them is misguided. To redirect the algorithm to focus on the cross-correlation among sensors, and not at the power levels, we normalized the measurements of each sensor so that the maximum amplitude of each sensor measurement is 1. With the normalized dataset, the weights corresponding to various look directions are as depicted in Figure 5. The resultant weights show that when the array is steered to endfire directions, sensor weights are more evenly distributed across the array. However, at array broadside look directions the weighting is more sparse. Regular striations are also visible for sensors 54 to 64, indicating that the broadband energy is centered at a frequency less than half the array design frequency (since every other element is underutilized in the weighting scheme).

## D. COMPARISON OF NADSB AND MVDR BEAMPATTERNS

Figure 6(A) compares the beampatterns of MVDR and NADSB for 1 second of real data. The number of snapshots is 39. The MVDR weights are based on a single temporal frequency data where the frequency is 4400 *Hz*. Since the number of snapshots is less than the number of sensors, the MVDR degenerates in this case. The NADSB is based on frequencies ranging from 50 Hz to 4050 Hz. The dotted black line corresponds to the look direction 117.6132° or $u = -0.4635$. The gain at $u = -0.4635$ is -12 dB for MVDR and -17.5 dB for NADSB. When a discrete interferer is added at $u = -0.4635$, the MVDR and NADSB beampatterns change to the beampatterns shown in Figure 6(B). The MVDR still fails because of the low number of snapshots while the NADSB adapts to the discrete noise. Note that the NADSB sidelobe levels decrease by about 10 dB over large directional swath, which results from the broadband design of NADSB to account for a broadband interferer. The gain at $u = -0.4635$ reduces to -29 dB thereby suppressing the discrete interferer substantially (by 11.5 dB). Hence, the NADSB shows the ability to adapt to noise and suppress it even in a snapshot-deficient scenario. Figure 6(C) compares the beampatterns of MVDR and NADSB for 10 seconds of real data (compare to Figure 6(A)). The number of snapshots is 390. The MVDR does not demonstrate good resolution despite the increase in number of snapshots. The gain at $u = -0.4635$ is -3 dB for MVDR and -22 dB for NADSB. When a discrete interferer is added at $u = -0.4635$, the MVDR and NADSB beampatterns change to the beampatterns shown in Figure 6(D). The MVDR now possesses high resolution and the ability to suppress the interferer by providing attenuation of -32 dB at the interferer location. However, the NADSB still outperforms the MVDR by providing an attenuation of -40 dB at the interferer location. Overall, the experimental results presented here demonstrate the superiority of the NADSB algorithm compared to MVDR.

V. OPTIMAL SENSOR LOCATIONS FOR A SPARSE ARRAY
The NADSB algorithm is well suited for modifications to find sensor locations that maximize the deflection coefficient for fixed aperture, number of sensors, and shading. Consider the
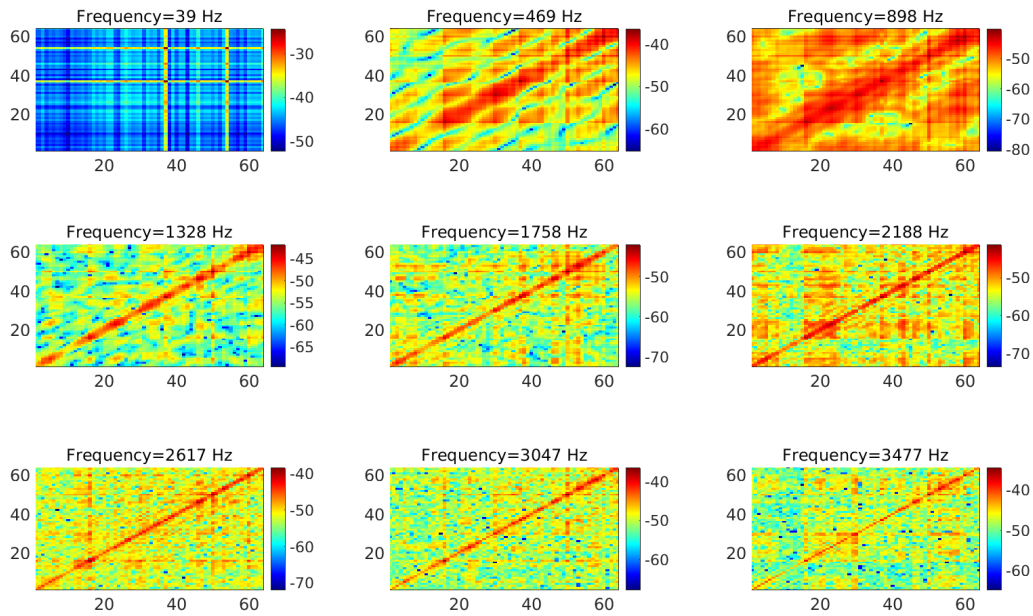
FIGURE 2. Cross power spectral density estimates among various sensors at 9 equally spaced frequencies. The x- and y-labels indicate sensor indices.
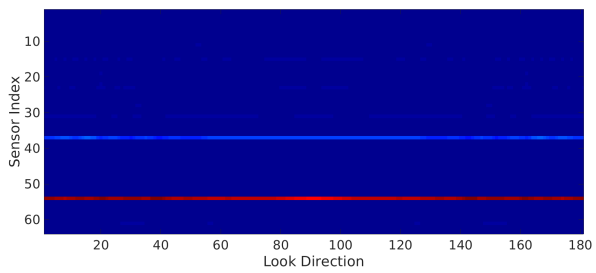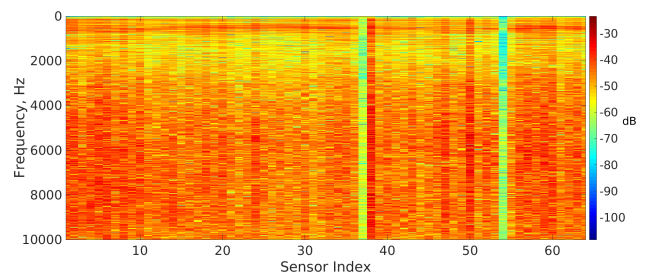

FIGURE 3. Optimum shadings for a 64-sensor array for 181 different look directions.
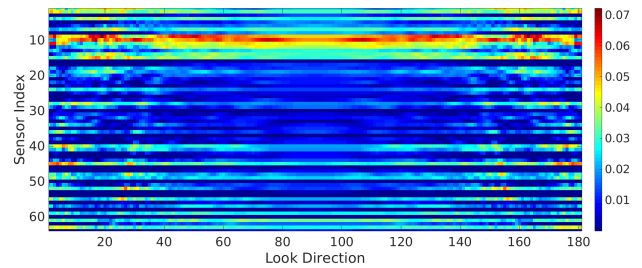

FIGURE 4. Temporal power spectral density estimate of the measured data.

sensor location grid for an *L*-sensor ULA, where the total number of sensors spanning the full aperture is *N*. The reformulated NADSB optimization problem can be expressed as

$$\min_{\mathbf{w}} \quad \mathbf{w}^T \left(\int_{\omega_1}^{\omega_2} \mathbf{U}^*(\omega)\mathbf{M}(\omega)\mathbf{U}(\omega)d\omega \right) \mathbf{w}$$

$$\text{subject to } \Sigma_{m=1}^{L} w_m = 1,$$

$$w_m = 0 \text{ or } 1/N, \quad \text{for } m = 2, 3, 4, \ldots, L-1,$$

$$w_1 = 1/N, \text{ and}$$

$$w_L = 1/N. \tag{18}$$

This is an optimization problem where the objective variables can only take values from a pre-defined discrete set. We used a genetic algorithm solver in MATLAB to solve this problem for $L = 57$ and $N = 21$ for the available dataset. With $L = 57$ and $N = 21$, we also form a coprime array, a nested array, and a semi-coprime array with subarray parameters as listed in Table 2. The arrays are depicted in Figure 7. Solving the optimization problem for 19 different look directions yielded the sensor locations


FIGURE 5. Optimum shadings for a 64-sensor array for 181 different look directions.

depicted in Figure 8. The optimal locations are look direction dependent. None of the 19 arrangements can be construed as a coprime, nested, or a semi-coprime array. Figure 9 verifies that the objective function in (15) is minimized by the optimal geometry obtained from the NADSB algorithm. The objective function values at all directions ranging from 0° to 180° are higher for the three sparse array geometries. This suggests that, from an information theory perspective, existing sparse
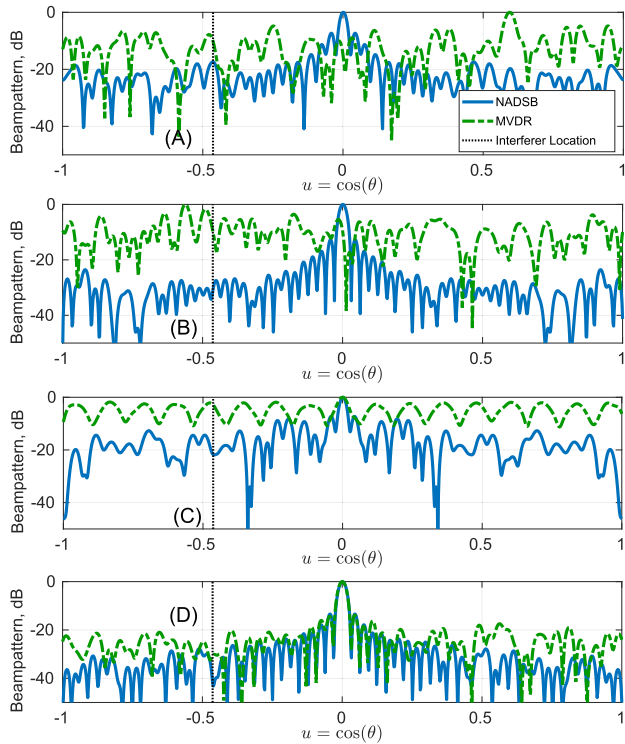
FIGURE 6. Comparison of NADSB and MVDR beampatterns. (A) Using 1 second of real data which resulted in 39 snapshots. (B) Using 1 second of real data with an injected discrete interferer. (C) Using 10 seconds of real data which resulted in 390 snapshots. (D) Using 10 second of real data with an injected discrete interferer.
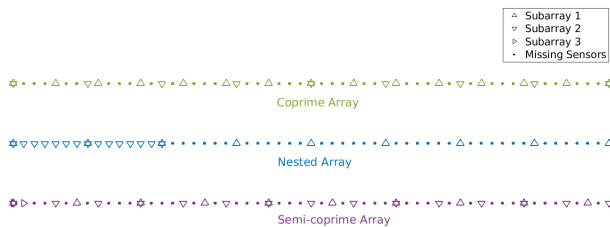
FIGURE 7. Sparse array geometries.

array designs are not naturally optimized. Further inclusion of min and product processing into the optimization algorithm may provide additional insights, which is an area of ongoing investigation.

Figure 10 further depicts the advantage of the optimal sensor locations over coprime, nested, and semi-coprime geometries. The beampatterns steered to $u = 0$ for the optimal (black dotted line), coprime (green solid line), nested (blue dash-dot line), and semi-coprime (purple dashed line) are depicted in the figure. Note that while the array geometries were optimized using a modification of the NADSB algorithm, the beampatterns in the figure are generated using standard DSB. The top panel corresponds to the original Kona dataset. The beampattern levels at $u = 0.5$ (corresponding to $\theta = 60°$) in the top panel for the optimal, coprime,

TABLE 2. Sparse array design parameters.

|	Subarray 1	Subarray 2	Subarray 3
Coprime	Number of sensors = 15, Undersampling factor = 4	Number of sensors = 9, Undersampling factor = 7	
Nested	Number of sensors = 9, Undersampling factor = 7	Number of sensors = 14, Undersampling factor = 1	
Semi-coprime	Number of sensors = 10, Undersampling factor = 6	Number of sensors = 15, Undersampling factor = 4	Number of sensors = 2, Undersampling factor = 1

FIGURE 8. Optimal locations for a sparse array with 21 sensors on the grid of a 57-sensor full ULA for look directions 0° to 180°. The filled circles indicate sensor locations.
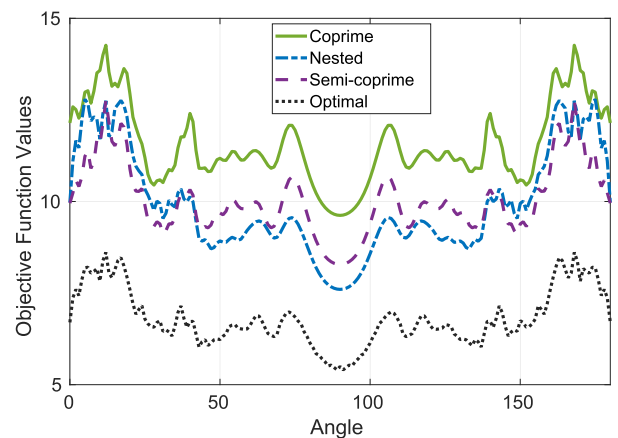
FIGURE 9. Objective function evaluated for sparse arrays in Figure 7 and the optimal array.

nested, and semi-coprime arrays are −14.64 dB, −4.103 dB, −19.98 dB, and −14.68 dB, respectively. An interferer with a bearing of $u = 0.5$ was added to the Kona dataset. The new set of sensor locations were found for the case with the interferer. The corresponding optimal beampattern is depicted in the bottom panel of the figure. The optimal beampattern value at $u = 0.5$ is −30.38 dB whereas the corresponding levels for the coprime, nested, and semi-coprime arrays are still −4.103 dB, −19.98 dB, and −14.68 dB, as expected. This example demonstrates higher capability of the optimal sparse array to reject interferers compared to the standard sparse
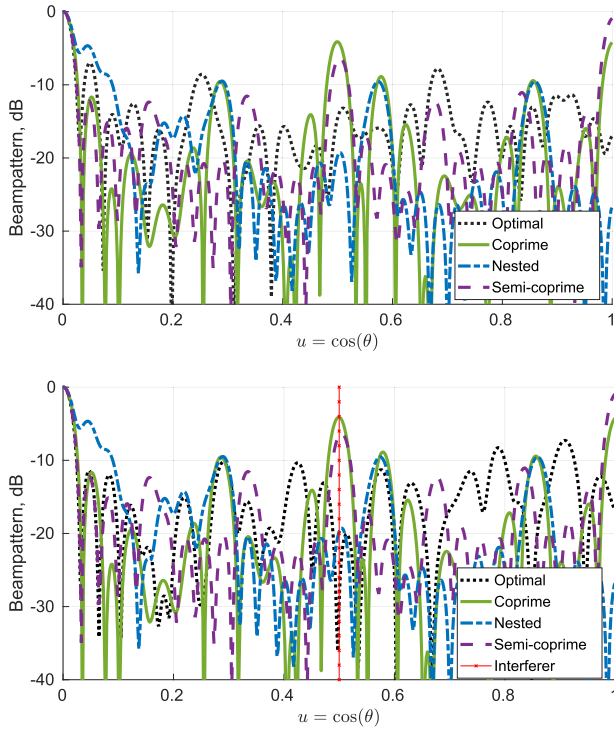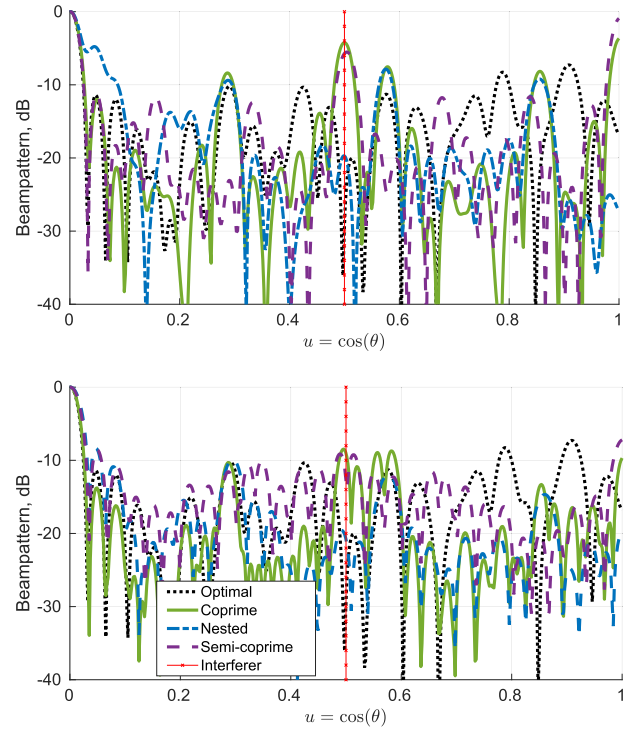
FIGURE 10. Beampatterns calculated using DSB for steering direction cosine of *u* = 0 and using (Top) noise only measurements and (Bottom) noise plus an injected interferer at *u* = 0.5. Results are shown using the optimal (black dotted line), coprime (green solid line), nested (blue dash-dot line), and semi-coprime (purple dashed line) array geometries.

FIGURE 11. Beampatterns generated using NADSB and applied by (Top) treating each array as a single nonuniform array and by (Bottom) treating each subarray component separately and using product processing with the results.

geometries, confirming the superiority of the optimal geometry over the three other sparse geometries in adapting to received signals.

VI. OPTIMAL WEIGHTS FOR STANDARD SPARSE ARRAYS

The NADSB algorithm is suitable for computation of optimal weights for any geometry. We used the NADSB algorithm to compute the optimal weights for the three sparse array geometries depicted in Figure 7. The optimal shading can be applied to these sparse geometries in two ways: (1) While evaluating these weights, each sparse array can be treated as a single non-uniform linear array and the NADSB weights for the sparse array can be found. The results are depicted in the top panel of Figure 11. (2) The optimal shading can be obtained for the individual subarrays of these sparse arrays. Then, product or min processing as described in [18]–[25] can be applied to these arrays. The beampatterns for product processing are shown in the bottom panel of Figure 11. The weights corresponding to all sparse geometries in Figure 11 are adaptive and are optimized to suppress a discrete interferer at *u* = 0.5. However, it is evident that the optimal array's beampattern (black dotted line) has higher attenuation at *u* = 0.5 than the coprime (green solid line), nested (blue dash-dot line), or the semi-coprime (purple dashed line) with optimal shadings obtained from the NADSB algorithm. This is true for both direct CBF of the sparse arrays treating them as single non-uniform linear arrays and CBFs for

individual subarrays followed by product or min processing. The examples presented in this section also show that the sparse arrays obtained using the NADSB algorithm provide higher suppression of interferers than coprime, nested, and semi-coprime arrays.

VII. CONCLUSION

In this paper we applied the noise adaptive beamforming algorithm, NADSB, to an underwater dataset obtained from a linear array and obtained the optimal shading for CBF. We compared the NADSB beampattern with MVDR by adding a discrete interferer to the available dataset and comparing the interferer suppression ability of the two algorithms. Our results showed that the NADSB provides greater attenuation of interferers when there are sufficient number of snapshots. Additionally, we showed that in a snapshot-deficient scenario, when the MVDR degenerated, the NADSB algorithm was still functional and able to suppress an interferer. Hence, the examples showed the superiority of the NADSB over MVDR and demonstrated the capability of the NADSB to work with fewer snapshots.

We also formulated the NADSB algorithm to find the optimal sparse geometry for a given number of sensors and aperture. Our results showed that the optimal sparse geometry and standard sparse geometries have significantly different beampatterns. The proposed sparse array geometry, which is yielded by the NADSB algorithm, provides

significantly better interferer rejection than coprime, nested, and semi-coprime arrays with the same number of sensors and aperture.

APPENDIX A
DERIVATION OF THE OPTIMAL WEIGHTS FOR UNCORRELATED NOISE

When the noise measurements are uncorrelated across different sensors, the matrix $\mathbf{M}(\omega)$ in (15) is diagonal. Since $\mathbf{U}^*(\omega)$ and $\mathbf{U}(\omega)$ are also diagonal, the product $\mathbf{U}^*(\omega)\mathbf{M}(\omega)\mathbf{U}(\omega)$ is an L-by-L diagonal matrix. The mth diagonal elements of $\mathbf{U}^*(\omega)$, $\mathbf{M}(\omega)$ and $\mathbf{U}(\omega)$ are $e^{-j\mathbf{k}_s.\mathbf{x}_m}$, $\tilde{\alpha}_m(\omega)$, and $e^{j\mathbf{k}_s.\mathbf{x}_m}$, respectively, where $\tilde{\alpha}_m(\omega)$ denotes the noise power at sensor m and frequency ω. Therefore, the mth diagonal element of $\mathbf{U}^*(\omega)\mathbf{M}(\omega)\mathbf{U}(\omega)$ is $\tilde{\alpha}_m(\omega)$. The matrix $\mathbf{J}$ is given by

$$\mathbf{J} = \begin{bmatrix} \int_{\omega_1}^{\omega_2} \tilde{\alpha}_1(\omega)d\omega & 0 & 0 \ldots & 0 \\ 0 & \int_{\omega_1}^{\omega_2} \tilde{\alpha}_2(\omega)d\omega & 0 \ldots & 0 \\ \vdots & \vdots & \vdots \ddots & \vdots \\ 0 & 0 & 0 \ldots & \int_{\omega_1}^{\omega_2} \tilde{\alpha}_L(\omega)d\omega \end{bmatrix}. \tag{19}$$

Denoting $\int_{\omega_1}^{\omega_2} \tilde{\alpha}_m(\omega)d\omega$ by α_m, for $m = 1, 2, \ldots L$, we get

$$\mathbf{J} = \begin{bmatrix} \alpha_1 & 0 & 0 & \ldots & 0 \\ 0 & \alpha_2 & 0 & \ldots & 0 \\ \vdots & \vdots & \vdots & \ddots & \vdots \\ 0 & 0 & 0 & \ldots & \alpha_L \end{bmatrix}. \tag{20}$$

Substituting the diagonal $\mathbf{J}$ from (20) in the objective function in (15), we get

$$\mathbf{w}^T \mathbf{J} \mathbf{w} = \sum_{m=1}^{L} w_m^2 \alpha_m. \tag{21}$$

Consider the minimization problem

$$\min_{\mathbf{w}} \ \mathbf{w}^T \mathbf{J} \mathbf{w}$$
$$\text{subject to } \Sigma_{m=1}^{L} w_m = 1. \tag{22}$$

The Lagrangian corresponding to (22) is

$$\mathbf{w}^T \mathbf{J} \mathbf{w} = \sum_{m=1}^{L} w_m^2 \alpha_m + \Lambda(\Sigma_{m=1}^{L} w_m - 1), \tag{23}$$

where Λ is the Lagrange multiplier. Differentiating the Lagrangian with respect to the weights and Λ and setting each derivative to 0, we get the following set of equations

$$2w_1\alpha_1 + \Lambda = 0$$
$$2w_2\alpha_2 + \Lambda = 0$$
$$\vdots$$
$$2w_L\alpha_L + \Lambda = 0$$
$$\Sigma_{m=1}^{L} w_m = 1. \tag{24}$$

Therefore, $w_m = -\Lambda/(2\alpha_m)$ for $m = 1, 2, \ldots, L$. Substituting $w_m = -\Lambda/(2\alpha_m)$ in $\Sigma_{m=1}^{L} w_m = 1$, we get $\sum_{m=1}^{L} \frac{-\Lambda}{2\alpha_m} = 1$. Therefore, the Lagrange multiplier is

$$\Lambda = -\frac{1}{\sum_{m=1}^{L} \frac{1}{2\alpha_m}}. \tag{25}$$

The optimal weight obtained by substituting Λ in (24) is

$$w_k = \frac{1}{\alpha_k \sum_{m=1}^{L} \frac{1}{\alpha_m}}, \tag{26}$$

for $k = 1, 2, \ldots, L$. Since the vector $[\frac{1}{\alpha_1}, \frac{1}{\alpha_2}, \ldots, \frac{1}{\alpha_L}]$ can be represented as $\mathfrak{D}\{\mathbf{J}^{-1}\}$ and c_n denotes the sum of the elements of $\mathfrak{D}\{\mathbf{J}^{-1}\}$, we can write the optimal weight vector as

$$\mathbf{w}_{opt} = \frac{\mathfrak{D}\{\mathbf{J}^{-1}\}}{c_n}.$$

Note that the optimization problem in (22) does not include the constraints $w_k \geq 0$. However, each weight in (26) is guaranteed to be greater than or equal to 0 since α_k is the noise power at sensor k and is guaranteed to be non-negative.

REFERENCES

[1] D. Johnson and D. Dudgeon, *Array Signal Processing: Concepts and Techniques*. New York, NY, USA: Simon and Schuster, 1992.

[2] H. V. Trees, *Optimum Array Processing: Part IV of Detection, Estimation, and Modulation Theory*. New York, NY, USA: Wiley, 2002.

[3] T. A. Wettergren, J. P. Casey, and R. L. Streit, "A numerical optimization approach to acoustic hull array design," *J. Acoust. Soc. Amer.*, vol. 112, no. 6, pp. 2735–2741, Dec. 2002, doi: 10.1121/1.1518982.

[4] C. M. Traweek, "Optimal spatial filtering for design of a conformal velocity sonar," Ph.D. dissertation, Graduate Program Acoust., PA State Univ., State College, PA, USA, 2003.

[5] T. A. Wettergren and C. M. Traweek, "Optimization of conventional beamformer shading weights for conformal velocity sonar," *IEEE J. Ocean. Eng.*, vol. 30, no. 1, pp. 213–220, Jan. 2005.

[6] K. Adhikari and B. Drozdenko, "Symmetry-imposed rectangular coprime and nested arrays for direction of arrival estimation with multiple signal classification," *IEEE Access*, vol. 7, pp. 153217–153229, 2019.

[7] K. Adhikari, "Beamforming with semi-coprime arrays," *J. Acoust. Soc. Amer.*, vol. 145, no. 5, pp. 2841–2850, May 2019, doi: 10.1121/1.5100281.

[8] H. V. Trees, *Detection, Estimation and Modulation Theory, Part I*. New York, NY, USA: Wiley, 2001.

[9] A. Papoulis, *Probability, Random Variables, and Stochastic Processes* (McGraw-Hill Series in Electrical Engineering). New York, NY, USA: McGraw-Hill, 1991. [Online]. Available: http://opac.inria.fr/record=b1077486

[10] M. Simon, *Probability Distributions Involving Gaussian Random Variables: A Handbook for Engineers and Scientists* (International Series in Engineering and Computer Science). London, U.K.: Springer, 2007. [Online]. Available: http://books.google.com/books?id=zjJdP0CJUAYC

[11] S. Kay, *Fundamentals of Statistical Signal Processing: Detection Theory*, vol. 2. Englewood Cliffs, NJ, USA: Prentice-Hall, 1998.

[12] S. M. Kay, *Information-Theoretic Signal Processing and Its Applications*. Newport County, RI, USA: Sachuest Point Publishers, 2020.

[13] W. Peterson, T. Birdsall, and W. Fox, "The theory of signal detectability," *Trans. IRE Prof. Group Inf. Theory*, vol. 4, no. 4, pp. 171–212, Sep. 1954.

[14] R. Urick, *Principles of Underwater Sound*. New York, NY, USA: McGraw-Hill, 1983.

[15] Mathworks. *Optimization Toolbox*. Accessed: Feb. 4, 2021. [Online]. Available: https://www.mathworks.com/help/optim/ug/fmincon.html

[16] *High Tech, Inc.* Accessed: Nov. 5, 2020. [Online]. Available: http://www.hightechincusa.com/products/hydrophones/hti92wb.html

[17] Mathworks. *Fmincon*. Accessed: Feb. 4, 2021. [Online]. Available: https://www.mathworks.com/products/global-optimization.html

[18] K. Adhikari, J. R. Buck, and K. E. Wage, "Extending coprime sensor arrays to achieve the peak side lobe height of a full uniform linear array," *EURASIP J. Adv. Signal Process.*, vol. 2014, no. 1, pp. 1–17, Dec. 2014, doi: 10.1186/1687-6180-2014-148.

[19] K. Adhikari, J. R. Buck, and K. E. Wage, "Beamforming with extended co-prime sensor arrays," in *Proc. IEEE Int. Conf. Acoust., Speech Signal Process. (ICASSP)*, May 2013, pp. 4183–4186.

[20] K. Adhikari and J. R. Buck, "Gaussian signal detection by coprime sensor arrays," in *Proc. IEEE Int. Conf. Acoust., Speech Signal Process. (ICASSP)*, Apr. 2015, pp. 2379–2383.

[21] K. Adhikari and J. R. Buck, "Spatial spectral estimation with product processing of a pair of colinear arrays," *IEEE Trans. Signal Process.*, vol. 65, no. 9, pp. 2389–2401, May 2017.

[22] Y. Liu and J. R. Buck, "Detecting Gaussian signals in the presence of interferers using the coprime sensor arrays with the min processor," in *Proc. 49th Asilomar Conf. Signals, Syst. Comput.*, Nov. 2015, pp. 370–374.

[23] V. Chavali, K. E. Wage, and J. R. Buck, "Multiplicative and min processing of experimental passive sonar data from thinned arrays," *J. Acoust. Soc. Amer.*, vol. 144, no. 6, pp. 3262–3274, Dec. 2018.

[24] K. Adhikari and B. Drozdenko, "Design and statistical analysis of tapered coprime and nested arrays for the min processor," *IEEE Access*, vol. 7, pp. 139601–139615, 2019.

[25] K. Adhikari and J. R. Buck, "Gaussian signal detection with product arrays," *IEEE Access*, vol. 8, pp. 36256–36266, 2020.

THOMAS A. WETTERGREN (Senior Member, IEEE) received the B.S. degree in electrical engineering and the Ph.D. degree in applied mathematics from Rensselaer Polytechnic Institute, Troy, NY, USA. He is currently a Senior Research Scientist and the U.S. Navy Senior Technologist for operational and information science with the Naval Undersea Warfare Center. His research interest includes the use of applied mathematics to develop new methods for the planning, control, and optimization of complex and multi-agent systems. He was a recipient of the IEEE-USA Harry Diamond Award, the NAVSEA Scientist of the Year, and the Dolores Etter Award for Top Navy Scientists and Engineers.

KAUSHALLYA ADHIKARI (Member, IEEE) received the M.S. and Ph.D. degrees in electrical engineering from the University of Massachusetts at Dartmouth, Dartmouth, MA, USA, in 2012 and 2016, respectively. She is currently an Assistant Professor of electrical engineering with the University of Rhode Island. Her research interests include signal processing, sensor array processing, and information theory.

LAUREN A. FREEMAN received the B.S. degree (Hons.) in marine biology and geology from the University of Miami, in 2008, and the Ph.D. degree in oceanography from the UCSD, in 2013. She is currently an Oceanographer with the Naval Undersea Warfare Center, Newport, RI, USA. Her research interests include ambient biological soundscapes, human impacts on marine ecosystems, bio-physical interactions, and climate impacts on coastal oceans.

BLAINE M. HARKER received the B.S. (Hons.) and Ph.D. degrees in physics from Brigham Young University, in 2012 and 2017, respectively. He is currently a Scientist with the Naval Undersea Warfare Center, Newport, RI, USA. His research interests include array signal processing, underwater acoustics, and aeroacoustics.

SIMON E. FREEMAN received the B.E. degree (Hons.) in mechanical engineering and the B.S. degree in marine science from The University of Auckland, New Zealand, in 2006, and the Ph.D. degree in oceanography from the UCSD, in 2013. He is currently an Oceanographer with the Naval Undersea Warfare Center, Newport, RI, USA. His research interests include signal processing, hydrophone array design, and biological systems.

• • •